PHYSICAL REVIEW B VOLUME 55, NUMBER 7 15 FEBRUARY 1997-I

Optical functions of semiconductors beyond density-functional theory and random-phase approximation

V. I. Gavrilenko
Physics Department, Brooklyn College of CUNY, 2900 Bedford Avenue, Brooklyn, New York 11210
and Friedrich-Schiller-Universität, Institut für Festkörpertheorie und Theoretische Optik, Max-Wien-Platz 1, 07743 Jena, Germany

F. Bechstedt
Friedrich-Schiller-Universität, Institut für Festkörpertheorie and Theoretische Optik, Max-Wien-Platz 1, 07743 Jena, Germany

(Received 17 May 1996; revised manuscript received 23 August 1996)

The linear optical response of semiconductors has been studied beyond the density-functional theory with *ab initio* pseudopotentials and the random-phase approximation. Effects of the macroscopic local fields and the microscopic exchange-correlation interaction are included in the description of the optical spectra. Quasiparticle corrections to the single-particle energies have been added in the polarization function. Numerical calculations are performed for the group-IV materials Si, SiC, and diamond as model substances. In the static limit and in the low-frequency region, corrections due to the local fields reduce the dielectric function, whereas inclusion of the exchange-correlation interaction enhance the oscillator strengths. In the high-energy region these effect have a more complex character, and the signs of the relevant corrections change in dependence on the photon energy. The effects considered strongly modify the plasmon resonance in the energy-loss function. The results obtained are discussed in comparison with theoretical and experimental data available. [S0163-1829(97)05907-9]

I. INTRODUCTION

In the past few years, a number of highly accurate calculations of optical and dielectric properties of semiconductors have appeared.[1–6] In general they are based on the independent-particle approximation[7–9] [often called the random-phase approximation (RPA)] and a first-principles description of the electronic and atomic structure in the framework of the density-functional theory (DFT) (Ref. 10) in the local-density approximation (LDA).[11] In some cases partially exchange-correlation (XC) effects have been taken into account. The independent-quasiparticle (QP) approximation[3,12] has been also introduced. First attempts[3] have been made to go beyond the RPA considering XC corrections. Local-field (LF) effects[8,9] due to the atomic structure of the matter influence the resulting optical spectra. In earlier works in the field[13–19] (and references therein), local-field and excitonic effects have already been discussed on the basis of the empirical-pseudopotential method or expansions of the eigenfunctions in terms of localized orbitals. In contrast to the discussion of complete optical spectra, the influence of local-field effects has been more extensively discussed in the case of dielectric properties, in particular for the macroscopic electronic dielectric constant ε_∞.[20–28]

In the present paper the influence of local-field effects as well as of exchange-correlation effects beyond the RPA is studied in detail for optical spectra of semiconductors. In addition we discuss XC self-energy effects,[6,24] i.e., quasiparticle (QP) shifts of the electron and hole DFT-LDA energies. As model substances the group-IV materials diamond (C), silicon (Si), and silicon carbide (SiC) crystallizing in diamond or zinc-blende structures are considered. SiC allows the study of the interplay of partially ionic bonding and the effects under consideration. The paper is organized as follows. Section II contains a brief summary of the theory of the macroscopic dielectric function. Computational details are outlined in Sec. III. The results are discussed and compared with those of other authors or experiments in Sec. IV. Section V contains a summary and conclusions.

II. MACROSCOPIC DIELECTRIC FUNCTION

A. Relation to microscopic dielectric function

According to Adler[8] and Wiser[9] the macroscopic dielectric function, $\varepsilon^M(\hat{\mathbf{q}};\omega)$, that governs the optical properties of a crystal,[29] may be directly related to the zeroth element of the inverse of the microscopic dielectric matrix $\varepsilon(\mathbf{q}+\mathbf{G},\mathbf{q}+\mathbf{G}';\omega)$, where $\mathbf{q}$ denotes a vanishing wave vector with direction $\hat{\mathbf{q}}$, and $\mathbf{G}$, and $\mathbf{G}'$ represent elements of the reciprocal Bravais lattice of the crystal. The zeroth element of the inverse dielectric matrix is influenced by the off-diagonal elements of the dielectric matrix.[30] They are due to the lattice periodicity and generate ''umklapp'' processes in the dielectric response. They are generally referred to as ''local-field effects.''[4,8,9,31] We define these LF effects more exactly as the discrepancy between $\varepsilon^M(\hat{\mathbf{q}};\omega)$ and the zeroth element of the dielectric matrix, $\lim_{\mathbf{q}\to 0}\varepsilon(\mathbf{q},\mathbf{q};\omega)$.

The microscopic dielectric matrix $\varepsilon(\mathbf{q}+\mathbf{G},\mathbf{q}+\mathbf{G}';\omega)$ is directly related to the polarization function $P(\mathbf{q}+\mathbf{G},\mathbf{q}+\mathbf{G}';\omega)$ of the system under consideration. It contains the irreducible diagrams of the proper part of the two-particle Green function.[32]

B. Exchange-correlation effects

If XC effects on the longitudinal response are not neglected, e.g. within the DFT or DFT-LDA, the polarization function P appears instead that of independent particles P_0.

It can be easily proved[4,21,25,33,34] that the expression for interacting particles takes the form

$$P(\mathbf{q}+\mathbf{G},\mathbf{q}+\mathbf{G}';\omega)=\sum_{\mathbf{G}''}\Gamma(\mathbf{q}+\mathbf{G},\mathbf{q}+\mathbf{G}'';\omega)\times P_0(\mathbf{q}+\mathbf{G}'',\mathbf{q}+\mathbf{G}';\omega), \tag{1}$$

where the matrix Γ is related to the vertex function of the system. The inverse matrix is given as

$$\Gamma^{-1}(\mathbf{q}+\mathbf{G},\mathbf{q}+\mathbf{G}';\omega)=\delta_{\mathbf{G}\cdot\mathbf{G}'}-\sum_{\mathbf{G}''}P_0(\mathbf{q}+\mathbf{G},\mathbf{q}+\mathbf{G}'';\omega)\times K_{\mathrm{XC}}(\mathbf{q}+\mathbf{G}'',\mathbf{q}+\mathbf{G}';\omega). \tag{2}$$

The kernel K_{XC} in this equation describes the XC effects taken into the two-particle function beyond the RPA. Within the DFT it may be represented in real space by $K_{\mathrm{XC}}=\delta^2E_{\mathrm{XC}}/(\delta n\,\delta n')$, with the electron density $n(\mathbf{x})$ and the total XC energy E_{XC}.[21,25] Practically the same result follows within the so-called time-dependent local-density approximation.[3,35] Within the DFT-LDA the kernel is local in real space, and does not depend on the frequency. Its diagonal part is constant. This LDA behavior is, generally speaking, incorrect. However, K_{XC} always appears in a product P_0K_{XC}. Thus the $\mathbf{q}$ dependence of P_0 damps the small-$\mathbf{q}$ contributions, although more slowly than in real systems.

C. Optical limit

The $\mathbf{q}\rightarrow 0$ limit is required to obtain the macroscopic dielectric function for optical applications. This limit has to be taken with care to keep the correct analytical properties of this function and the underlying inverse dielectric matrix.[36] This may be reached by the direct diagonalization of the dielectric matrix. The procedure for the zeroth element, which is of interest here, has been described by Pick, Cohen, and Martin.[36] As a result the longitudinal macroscopic dielectric function is derived to be

$$\varepsilon^M(\hat{\mathbf{q}};\omega)=\lim_{\mathbf{q}\rightarrow 0}\left\{\varepsilon(\mathbf{q},\mathbf{q};\omega)-\sum_{\mathbf{G},\mathbf{G}'(\neq 0)}\varepsilon(\mathbf{q},\mathbf{G};\omega)\times S^{-1}(\mathbf{G},\mathbf{G}';\omega)\varepsilon(\mathbf{G}',\mathbf{q};\omega)\right\}, \tag{3}$$

where S^{-1} is the inverse of the lower-right submatrix of $\varepsilon(\mathbf{q}+\mathbf{G},\mathbf{q}+\mathbf{G}';\omega)$ corresponding to nonzero reciprocal-lattice vectors $\mathbf{G}$ and $\mathbf{G}'\neq 0$, the so-called ''body'' of the dielectric matrix.[25] This submatrix is always an analytical function of $\mathbf{q}$, even at $\mathbf{q}=0$. Therefore, the limit $\mathbf{q}\rightarrow 0$ can be taken from the very beginning. The same holds partially for the ''wing'' elements $\varepsilon(\mathbf{q},\mathbf{G};\omega)$ and $\varepsilon(\mathbf{G},\mathbf{q};\omega)$ of the dielectric matrix. However, their remaining wave-vector dependence and the wave-vector dependence of the ''head'' $\varepsilon(\mathbf{q},\mathbf{q};\omega)$ of the matrix govern the analytic properties of the macroscopic dielectric function. The second term on the right-hand side represents the local-field corrections to the macroscopic dielectric function, whereas the first term corresponds to the response in a nearly homogeneous system. Representation (3) allows two important conclusions. First, assuming that the diagonal elements give rise to the main contributions, LF effects should reduce the result $\varepsilon(\mathbf{q},\mathbf{q};\omega)$ of the diagonal approximation. Second, when the kernel K_{XC} is taken within the DFT-LDA, the XC effects only influence the LF corrections. The result of the diagonal approximation $\varepsilon(\mathbf{q},\mathbf{q};\omega)$ is not influenced.

The limit $\mathbf{q}\rightarrow 0$ can be explicitly performed in expressions (1)–(3) using the relation[6]

$$\langle c\mathbf{k}|e^{i\mathbf{q}\cdot\mathbf{x}}|v\mathbf{k}'\rangle=\hbar\mathbf{q}\frac{\langle c\mathbf{k}|\mathbf{v}|v\mathbf{k}\rangle}{\epsilon_c(\mathbf{k})-\epsilon_v(\mathbf{k})}\delta_{\mathbf{k}\cdot\mathbf{k}'}, \tag{4}$$

where the velocity operator $\mathbf{v}=i/\hbar[H,\mathbf{x}]_-$ belonging to the single-particle Hamiltonian H is introduced. Since the Hamiltonian has the formal structure $H=\mathbf{p}^2/2m+V_l+V_{\mathrm{nl}}$, where the total potential, $V=V_l+V_{\mathrm{nl}}$, is divided into a local (l) and a nonlocal (nl) part, the velocity operator $\mathbf{v}$ cannot be replaced by the momentum operator $\mathbf{p}/m$. Rather a correction term $\sim V_{\mathrm{nl}}$ appears. Typical origins of such nonlocalities are the nonlocal pseudopotentials used to describe the electron-ion interaction.[37] Here Bloch integrals of exponential functions with the Bloch eigenfunctions $|n\mathbf{k}\rangle$ belonging to the bandindex n, the wave vector $\mathbf{k}$ from the Brillouin zone (BZ), and the single-particle energy $\epsilon_n(\mathbf{k})$ are introduced. Within the DFT-LDA treatment[10,11] of the electronic structure $\epsilon_n(\mathbf{k})$ and $|n\mathbf{k}\rangle$ are solutions of the Kohn-Sham equations. For the considered semiconductors, the Bloch states will be taken to have occupancies of 0 (conduction bands $n=c$) or 1 (valence bands $n=v$).

The important elements of the dielectric matrix containing the $\mathbf{q}$ dependence may be rewritten by means of relation (4) what can be interpreted as a transformation from a longitudinal to a transverse electromagnetic perturbation.[6] For $\mathbf{q}\rightarrow 0$, the head element results into

$$\varepsilon(\mathbf{q},\mathbf{q};\omega)=\hat{\mathbf{q}}\cdot\underline{\varepsilon}(\omega)\cdot\hat{\mathbf{q}}, \tag{5}$$

with the tensor elements $(i,j=x,y,z)$ resulting from the matrix-element displacement in the polarization function for independent particles. Neglecting for simplicity the XC effects for a moment, the wing elements follow in the form

$$\varepsilon(\mathbf{q},\mathbf{G};\omega)=\hat{\mathbf{q}}\frac{|\mathbf{G}|}{|\mathbf{q}|}\mathbf{W}(\mathbf{G};\omega),$$

$$\varepsilon(\mathbf{G},\mathbf{q};\omega)=\frac{|\mathbf{q}|}{|\mathbf{G}|}\mathbf{W}^*(\mathbf{G};-\omega)\hat{\mathbf{q}}, \tag{6}$$

with $(j=x,y,z)$

$$W_j(\mathbf{G};\omega)=\frac{16\pi e^2\hbar}{|\mathbf{G}|V}\times\sum_{\mathbf{k}}\sum_{c,v}\frac{\langle c\mathbf{k}|e^{i\mathbf{G}\cdot\mathbf{x}}|v\mathbf{k}\rangle\langle v\mathbf{k}|v_j|c\mathbf{k}\rangle}{[\epsilon_c(\mathbf{k})-\epsilon_v(\mathbf{k})]^2-\hbar^2(\omega+i\eta)^2}. \tag{7}$$

Consequently, the longitudinal macroscopic dielectric function transforms into

$$\varepsilon^M(\hat{\mathbf{q}};\omega)=\hat{\mathbf{q}}\cdot\underline{\varepsilon}^M(\omega)\cdot\hat{\mathbf{q}}, \tag{8}$$

TABLE I. Convergence of ε_∞ including local-field effects as well as nonlocality of the velocity operator as a function of the number of conduction bands N_{CB}. The XC effects are omitted. For comparison values without LF effects ($N_{\mathrm{CB}}=176$) and experimental values (Ref. 41) are also listed.

Material	No LF	$N_{\mathrm{CB}}=16$	$N_{\mathrm{CB}}=56$	$N_{\mathrm{CB}}=76$	$N_{\mathrm{CB}}=96$	$N_{\mathrm{CB}}=116$	$N_{\mathrm{CB}}=176$	Expt.
Si	14.29	12.42	11.91	11.83	11.81	11.80	11.80	11.7
SiC	7.77	6.86	6.76	6.69	6.65	6.63	6.63	6.7
C	6.72	5.92	5.81	5.78	5.76	5.75	5.74	5.7

with the macroscopic optical tensor

$$\varepsilon_{ij}^{M}(\omega)=\varepsilon_{ij}(\omega)-\sum_{\mathbf{G},\mathbf{G}'(\neq 0)}\frac{|\mathbf{G}|}{|\mathbf{G}'|}W_i(\mathbf{G};\omega)S^{-1}(\mathbf{G},\mathbf{G}';\omega)\times W_j^{*}(\mathbf{G}';-\omega). \tag{9}$$

The relation of the macroscopic dielectric function in expression (8) to the second-rank tensor $\underline{\varepsilon}^{M}(\omega)$ indicates that we have indeed introduced the longitudinal function. The tensor $\varepsilon^{M}(\omega)$ also determines the transverse dielectric function $\mathbf{e}\cdot\underline{\varepsilon}^{M}(\omega)\cdot\mathbf{e}$, with a unit vector $\mathbf{e}=\mathbf{e}(\mathbf{q})\perp\hat{\mathbf{q}}$. For cubic crystals the tensor is diagonal, $\varepsilon_{ij}^{M}(\omega)=\varepsilon^{M}(\omega)\delta_{ij}$, with equal components independent of the choice of the Cartesian coordinate system. Consequently, the macroscopic longitudinal and transverse dielectric functions are equal in the limit of vanishing photon wave vectors,[29] and $\varepsilon_\infty=\varepsilon^{M}(0)$ defines the macroscopic electronic dielectric constant of the system.

III. TECHNICAL DETAILS

A. Electronic band-structure calculation

The electronic-structure calculations underlying the computations of the optical properties are based on the DFT-LDA.[38] The electron-ion interaction is treated by norm-conserving, *ab initio*, fully separable pseudopotentials in the Kleinman-Bylander form.[39] They are based on relativistic all-electron calculations for the free atoms by solving the Dirac equation self-consistently. As model systems we consider silicon- and carbon-based crystals. The C potentials are softened by careful choosing of the core radii.[40] The electronic wave functions are expanded in terms of plane waves. The energy cutoffs for the plane-wave expansion are chosen to 15, 34, and 42 Ry for silicon (Si), silicon carbide (SiC), and diamond (C). They are sufficient for converged total-energy and lattice-constant calculations. The total-energy optimizations give rise to theoretical cubic lattice constants of $a=10.227$ a.u. for Si, $a=8.109$ a.u. for SiC, and $a=6.681$ a.u. for C. They are used, although they slightly underestimate the experimental ones,[41] and, hence, somewhat enlarge the DFT-LDA transition energies. We also study the influence of many-body QP effects. Thereby we usually overcome the scissors-operator approximation.[3,6,12,24] The QP corrections to the DFT-LDA eigenvalues are computed within the GW approximation for the XC self-energy[24] according to a simplified scheme developed by Cappellini and co-workers.[42–44]. Using the numerical input described above corresponding shift values have been published for Si and diamond in Ref. 6, and for SiC in Ref. 44. The problems accompanying the inclusion of wave-vector- and band-index-dependent quasiparticle shifts beyond the scissors-operator approximation were discussed by us in detail in Ref. 6. The wave functions are identified with those obtained from the DFT-LDA. Consequently, the optical transition matrix elements are fixed at the corresponding values. The dynamical effects on the spectral distributions of the excited electrons and holes are neglected. Only the DFT-LDA energies in the spectra are replaced by such energies shifted by wave-vector- and band-index-dependent many-body corrections $\Delta_n(\mathbf{k})$. These corrections vary remarkably. For instance, for SiC we observe a considerable variation. In the upper valence bands $\Delta_n(\mathbf{k})$ varies from 0.0 eV (Γ_{15}) to about 1.4 eV (X_1, L_1). The shifts of the lower conduction bands with about 1.4 eV are rather independent. The variations are only of the order of 0.1 eV. However, for the higher conduction bands (X_5, L_1) there is an increase to about 2.0 eV (or more) at the zone boundaries.

The XC effect of the electron-electron interaction is described within the LDA, where the XC energy $\epsilon_{\mathrm{XC}}(n)$ per electron is replaced by that of a homogeneous electron gas. More precisely the Ceperley-Alder scheme[45] is used in a parametrization by Perdew and Zunger.[46] This parametrization is also the starting point for the determination of the XC response kernel K_{XC}. This approximate kernel is applied throughout the paper, i.e., also in the case of the calculations where QP effects are described by wave-vector- and band-index-dependent shifts.

B. Convergence

A crucial point of the calculations concerns the number of conduction bands N_{CB} and the rank $N_{\mathbf{G}}$ of the microscopic dielectric matrix taken into account. The convergence properties of the head, wing, and body elements with increasing N_{CB} are rather different. The reason of the different convergence properties is related to the different dependences on the band structure.[20] For example, in the static case it nearly holds that $\varepsilon(\mathbf{q}+\mathbf{G},\mathbf{q}+\mathbf{G}';0)\sim[\epsilon_c(\mathbf{k})-\epsilon_v(\mathbf{k})]^{-\nu}$ with $\nu=3$ (2;1) for $\mathbf{G}=\mathbf{G}'=0$ ($\mathbf{G}=0$, $\mathbf{G}'\neq 0$ or $\mathbf{G}\neq 0$, $\mathbf{G}'=0$; $\mathbf{G},\mathbf{G}'\neq 0$). Consequently, the convergence is determined by the body elements. Small numbers of conduction bands, e.g., $N_{\mathrm{CB}}=4$, which give already a reasonable frequency dependence in the diagonal case,[6] are insufficient. This is clearly shown by Table I for the macroscopic dielectric constant ε_∞. Many more bands are needed. In the computations of the frequency dependences, we use numbers $N_{\mathrm{CB}}=176$ (Si, SiC, C), which give converged results.

The influence of the size of the dielectric matrix that has to be inverted is indicated in Fig. 1 for the macroscopic dielectric constant. In the corresponding calculation for C, SiC, and Si, we included sets of $\mathbf{G}$ vectors through (000),

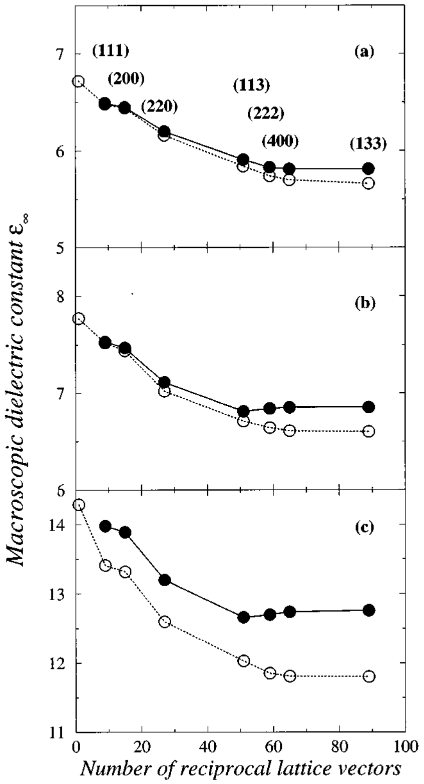

FIG. 1. Macroscopic dielectric constant $\varepsilon_\infty = \varepsilon^M(0)$ for diamond (a), silicon carbide (b), and silicon (c) vs the number of **G** vectors taken into account. Circles (dotted line): including the pure effect of local-field corrections; dots (solid line): the effect of the XC kernel K_{XC} is included in addition.

(111), (200), (220), (113), (222), (400), and (133), respectively. This means that the maximum matrix size considered is $N_{\mathbf{G}} = 89$. From Fig. 1 we conclude that a reasonable convergence is already obtained for a restriction up to **G** vectors of the type (113), independently of the inclusion of the XC kernel in addition to the LF effects or not. The limitation to **G** vectors shorter than the (222) ones corresponds to a restriction to the fifth-nearest-neighbor shell in the reciprocal Bravais lattice. The rank of the matrix in this case is $N_{\mathbf{G}} = 59$. Calculating only ε_∞, Baroni and Resta[23] considered up to 181 reciprocal-lattice vectors. However, here we have to calculate complete spectra, including absorption contributions. Thus, in order to make the computational time tolerable, the optical functions are evaluated with the mentioned restriction.

The sufficient number N_{CB} of conduction bands depends on the reciprocal-lattice vectors **G** included in the dielectric matrix. Baldereschi and Tosatti[20] already discussed that the large $\mathbf{G}, \mathbf{G}'$ components of the dielectric matrix are dominated by Bloch integrals connecting the valence bands to high-lying conduction bands. Hybertsen and Louie[25] concluded that N_{CB} must be on the order of double the size of the rank of the considered dielectric matrix to achieve numerical convergence of all the elements of the matrix to within a few percent. Our choice of $N_{\mathrm{CB}} = 176$ and $N_{\mathbf{G}} = 59$ indicates a similar conclusion.

C. Brillouin-zone integration

A crucial point of the explicit numerical calculations of the macroscopic dielectric function concerns the BZ integration. It should be reduced to the smallest possible part, for instance to the irreducible part of the BZ (IBZ), i.e., $\frac{1}{48}$th part of the BZ in the fcc case under consideration. This is in general not possible. Since the matrix $\varepsilon(\mathbf{q}+\mathbf{G}, \mathbf{q}+\mathbf{G}'; \omega)$ has the symmetry of the little group $g_{\mathbf{q}}$ of the wave vector **q**, the degree of the BZ-integration reduction depends on **q**. To achieve maximum computational efficiency, we make full use of the symmetry under consideration.

Critical points of the IBZ integration concern the dense of the **k**-point mesh and the type of the integration. It has been proved previously,[20,23,25] that, in the calculation of the static dielectric constant, a good convergence is achieved by the use of a relatively small number $N_{\mathbf{k}}$ of special **k** points. Typical numbers $N_{\mathbf{k}}$ are not very much larger than 10. However, calculating the whole spectra of $\mathrm{Re}\varepsilon^M(\omega)$ and $\mathrm{Im}\varepsilon^M(\omega)$, many more points are needed.[15] The reason is that the antisymmetric part of a matrix element $\varepsilon_A(\mathbf{q}+\mathbf{G}, \mathbf{q}+\mathbf{G}'; \omega)$ is proportional to a Dirac's δ function in the energy. Daling, van Haeringen, and Farid[4] solve this problem by combining the special-point technique with a continued-fraction expansion of the polarization function. We apply a combination of the linear tetrahedron method,[47] and a special-point technique for the **k**-space integration. Because of the smallness of the wing and body elements of the dielectric matrix, the requirements for their accuracy are considerably lower than in the case of the $\mathbf{G} = \mathbf{G}' = 0$ element. The most important diagonal head contributions $\varepsilon_{jj}(\omega)$ are calculated within the tetrahedron method. More strictly speaking, their imaginary parts are integrated by means of this method, whereas the real parts are then obtained via a Kramers-Kronig relation. The involved frequency integration is performed numerically using discrete frequencies in a distance of 1 meV. We have shown[6] that $N_{\mathbf{k}} = 89$ is sufficient in the IBZ of the fcc BZ. For the wing and body elements we use 235 special-**k** points within the IBZ. To smooth the resulting spectra a Lorentzian broadening of $\eta = 0.1$ eV [cf. expression (7)] is introduced. We have checked that the results obtained with special-point numbers $N_{\mathbf{k}} \leqslant 44$ are not sufficient. The spectra reveal changes with increasing $N_{\mathbf{k}}$ in the high-frequency region. The use of $N_{\mathbf{k}} = 235$ for the calculation of the off-diagonal elements of the dielectric matrix seems to be a reasonable compromise.

IV. RESULTS AND DISCUSSION

A. Frequency dependence of microscopic dielectric matrix

The off-diagonal elements of the dielectric matrix represent the local-field effects. Important examples for wing and body matrix elements are represented in Fig. 2 for silicon. They amount to roughly a few percent of the values of the $\mathbf{G} = \mathbf{G}' = 0$ element.[6] In the $\omega = 0$ case one finds 4% for the wing $\mathbf{G} = (000)$, $\mathbf{G}' = (111)$, and 10% for the diagonal body element $\mathbf{G} = (111)$, $\mathbf{G}' = (111)$. These values are generally reduced for higher frequencies. The effect of the off-diagonal body elements is usually one order of magnitude smaller. The influence of the off-diagonal body elements [cf. $\mathbf{G} = (111)$ and $\mathbf{G}' = (200)$] is therefore rather limited. For discussion of the main LF effects the transformation matrix in expression (3) may be nearly replaced by $S^{-1}(\mathbf{G}, \mathbf{G}'; \omega) = \delta_{\mathbf{G} \cdot \mathbf{G}'} / \varepsilon(\mathbf{G}, \mathbf{G}'; \omega)$.

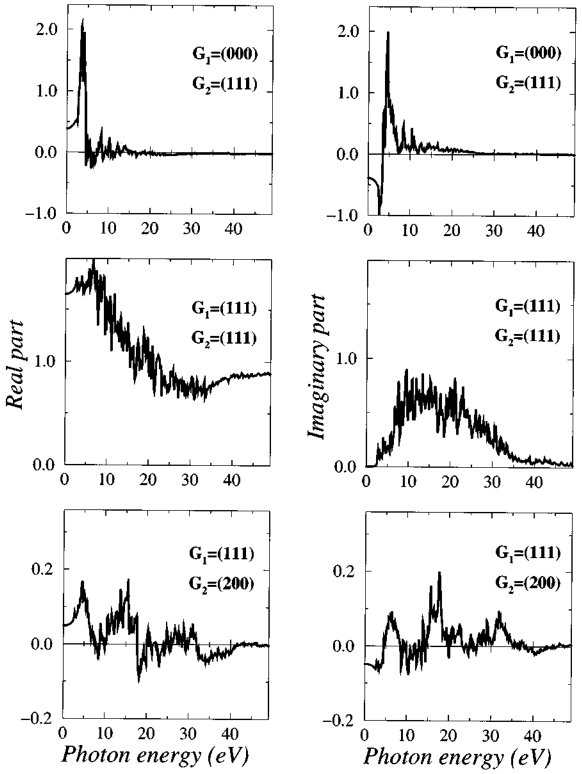

FIG. 2. One wing, diagonal body, and off-diagonal body element of the symmetrized dielectric matrix of silicon vs photon energy. The limit $\mathbf{q}\rightarrow 0 \| [100]$ is considered.

The small-frequency argument fails somewhat in the region of high photon energies $\hbar\omega$. Figure 2 indicates in the silicon case that for $\hbar\omega \gtrsim 20$ eV the head and wing elements practically vanish, whereas the diagonal body element makes a finite contribution. However, according to expression (3) the effect on the LF contributions to the macroscopic dielectric function remains small, since their magnitude is limited by the wing elements. This is clearly demonstrated in Fig. 3, where the LF contribution to the macroscopic dielectric function is plotted. One observes the well-known reduction of its real part in the static limit. However, the most important changes appear in the spectral region of the strongest optical transitions. They can be positive or negative. Consequently, no clear rules about the influence of LF corrections may be derived for the frequency region above the absorption edge. More in detail, the changes in this region exhibit an oscillator character. The oscillator frequencies may be related to characteristic optical transitions. In the silicon case, they are defined by that of the $E_1(E_0')$, E_2, and E_1' transitions. In the SiC (C) spectra one observes big changes close to the position of the main peaks in the absorption spectra related to E_0 and E_1 (E_2).[6]

B. LF and XC effects in the macroscopic dielectric function

In the static limit the influence of the effects under discussion are represented in Table II. LF effects strongly reduce the dielectric constant evaluated within the diagonal approximation by about 20%. When the XC kernel is also included, this reduction is partially lifted. It amounts only roughly 13%. The inclusion of the single-particle XC self-energy in the GW approximation beyond the DFT-LDA induces a further dramatic reduction. The reduction of the static dielectric constant due to the self-energy corrections has been reported for Si,[3] for diamond, and for SiC.[22] The resulting values are below the experimental ones. This happens although the wave-vector- and band-index-dependent QP corrections of the band energies are scaled down according to a procedure described in Sec. IV C. The necessity for such a remarkable reduction is already observed by Levine and Allan,[3] bringing the calculated values ε_∞ close to the experimental ones. The reason is, at the very least, a puzzle.

TABLE II. Influence of LF and XC effects on the macroscopic dielectric constant ε_∞. Starting point is the diagonal approximation. Successively the effects discussed (among them also wave-vector- and band-index-dependent QP shifts) have been included. For comparison experimental values (Ref. 41) are given.

Material	diagonal	+LF	+LF+XC	+LF+XC+QP	Expt.
Si	14.29	11.80	12.74	10.85	11.7
SiC	7.77	6.63	6.84	5.88	6.7
C	6.79	5.74	6.03	5.36	5.7

The frequency-dependent changes $\Delta\varepsilon^M(\omega)$ induced by LF and XC effects in the macroscopic optical functions are represented in Fig. 3. In general, the influence of the XC effects is remarkably smaller than that of the local fields. This is understandable from the fact that the influence of the XC kernel vanishes with the neglect of the LF. However, in contrast to the static case, where the XC inclusion reduces

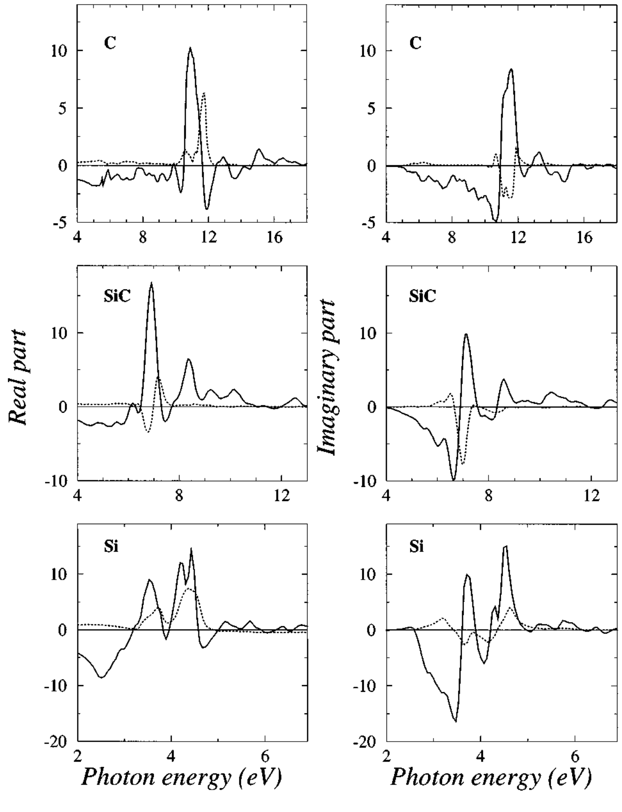

FIG. 3. Local-field (solid line) and exchange-correlation (dotted line) contributions to the macroscopic dielectric function vs photon energy for the three materials C, SiC, and Si.

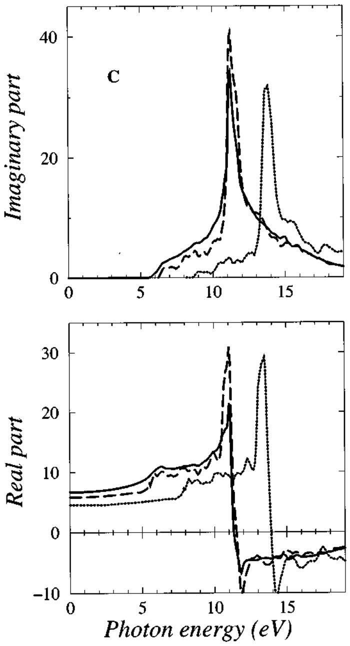

FIG. 4. Macroscopic dielectric function of diamond vs photon energy. Dashed line: without LF and XC effects (only $\mathbf{G}=\mathbf{G}'=0$ element); solid line: with LF and XC effects; dotted line: with LF and XC effects but shifted by wave-vector- and band-index-dependent QP corrections.

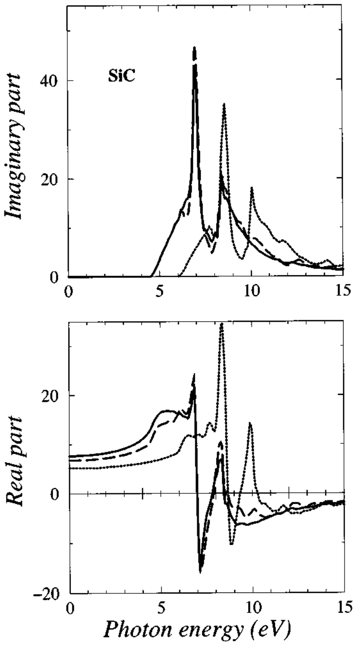

FIG. 5. As Fig. 4, but for silicon carbide.

the LF effects, the sign of the XC effect varies with the photon energy and is not clearly related to that of the LF effects. In the low-energy range, the signs of the real parts of $\Delta\varepsilon^M(\omega)$ induced by LF and XC effects are different. In the region of the main absorption peaks the situation of LF and XC effects is not unique. Whereas in the Si case the XC kernel strengthens the LF effects, the LF and XC influences are nearly opposite for the stronger bonded materials SiC and C. In the high-energy range, where direct optical transitions expire, the effect of the XC kernel is negligible in the real part as well as the imaginary part of the dielectric function. Positive and negative variations of the oscillator strengths occur in the imaginary parts due to local fields. In general, there is a reduction (increase) below (above) the main absorption peaks. The XC kernel acts only for photon energies close to the main absorption, and reduces the LF effects on average.

The macroscopic dielectric functions resulting for C, SiC, and Si are plotted versus photon energy in Figs. 4, 5, and 6 within different approximations: without LF and XC effects, with LF and XC effects, and with LF and XC effects but using QP eigenvalues instead of DFT-LDA ones. Curves, which represent LF effects separately, are not shown. The main effect can already be seen from the plots, including LF effects and the XC kernel. The nonlocality LF and many-body XC effects have practically no influence on the peak positions, but give rise to remarkable renormalizations of the oscillator strengths. Compared with the $\mathbf{G}=\mathbf{G}'=0$ element of the dielectric function, the LF effects reduce the oscillator strength in $\varepsilon^M(\omega)$ in the spectral region below the main absorption peaks. On the other hand, the inclusion of the XC kernel reduces the LF effects in this region. The corresponding curves lie in between those for $\varepsilon(\omega)$ and $\varepsilon^M(\omega)$ (only with LF but not shown). The net effect including the LF and XC amounts roughly to only 60% of the pure LF influence using the RPA expression for the polarization function.

The comparison of the spectra for C, SiC, and Si make it evident that the LF and XC effects show only weakly pronounced chemical trends with the averaged size of the atoms, the localization of the wave functions, or the averaged density of the electrons. The strongest LF and XC effects appear for silicon, whereas their relative influence is slightly reduced, changing to diamond. This result is in agreement with earlier calculations for Si and C.[14,15] A simple explanation of this trend arises from expression (3). Assuming that the magnitude of the wing and body elements of the dielectric matrix

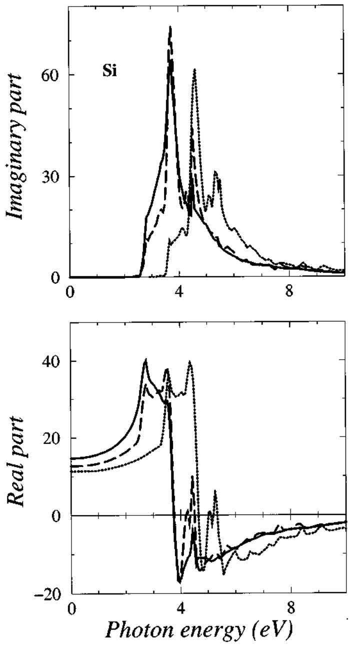

FIG. 6. As Fig. 4, but for silicon.

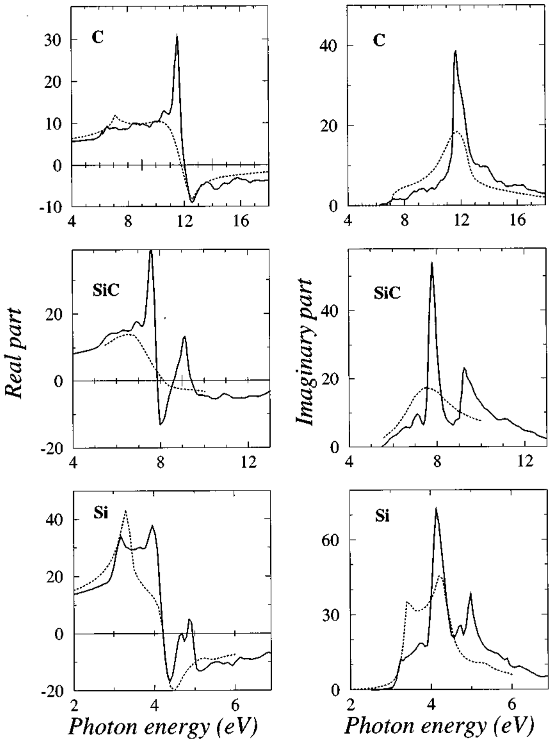

FIG. 7. Macroscopic dielectric function of diamond, silicon carbide, and silicon vs photon energy. Solid lines: calculated results including LF, XC, and QP effects; dotted lines: experimental results for Si (Ref. 48), SiC (Ref. 49) and diamond (Ref. 50).

scales with the electron density according to the generalized f-sum rule,[31] the local-field corrections are proportional to this density. However, the density is weighted by the inverse average gap of the system. As a consequence of the interplay of the two factors, the net effect of the local fields (or LF combined with XC effects) is absolutely and relatively weaker in the materials with stronger bonds.

C. Comparison with experiment

In Fig. 7 the macroscopic dielectric functions of C, SiC, and Si are calculated within the DFT-LDA but including LF, XC, and QP effects, and are compared with experimental data.[48–50] The theoretical spectra are shifted toward lower energies to bring the experimental and theoretical real parts closer together. For this purpose, the calculated QP shifts $\Delta_n(\mathbf{k})$ are replaced by $A\cdot\Delta_n(\mathbf{k})$, with scaling factors $A=0.2$ (C), 0.45 (SiC), and 0.5 (Si). This rescaling reduces the effect of the wave-vector- and band-index-dependent quasiparticle shifts calculated for Si, SiC, and C.[6,44] Considering the comparison of theoretical and experimental optical spectra over a wide range of photon energies, one can conclude that the QP effect is overestimated for the most important optical transition, e.g., E_1 and E_2 in Si and C, in contrast to electron-hole pair excitations near the fundamental indirect energy gap. Using the positions of the zero in the real parts of the macroscopic dielectric function in order to define averaged scissors operators Δ, one derives from the wave-vector- and band-index-dependent QP corrections values $\Delta=0.95$ (Si), 1.65 (SiC), and 2.65 eV (C). However, averaged scissors operators being necessary only amount to $\Delta=0.47$ (Si), 0.84 (SiC), and $\Delta=0.40$ eV (C). The reason for this observation is not very clear. One posssible reason could be related to excitonic effects which increase with the localization of the electronic states in the considered material. We mention that similarly small scissors operators have been found to bring the calcuations of ε_∞ into agreement with experiment.[3]

A general feature of the theoretical spectra for the imaginary part is that the overestimation of the intensity of the E_2 peak, i.e., the high-energy peak in $\mathrm{Im}\varepsilon^M(\omega)$, is reduced by the LF effects in the case of Si and C. This maximum is not more so sharply peaked as without LF and XC effects. However, the shoulder at the low-energy side of the theoretical spectra $\mathrm{Im}\varepsilon^M(\omega)$ is not enhanced. Only the inclusion of the Coulomb attraction between the electron and hole is expected to enhance the oscillator strengths in this spectral region drastically. In the case of SiC the double peak in the Im $\varepsilon^M(\omega)$ spectrum is related to optical transitions other than E_1 and E_2, due to the narrowing of conduction and valence bands around the X point in the Brillouin zone.[6] In principle, after inclusion of LF and XC effects the same happens as in the case of Si and C. It is obvious that, in the case of silicon and diamond, LF or LF and XC or LF, XC, and QP effects do not really improve the agreement of the theoretical spectra with measurement data. This holds especially for the low-energy E_1 peak in the imaginary part, which is additionally lowered with respect to the experimental intensities. To lift this discrepancy, the inclusion of excitonic effects is needed. On the other hand, the reduction of the strength of the high-energy E_2 peak seems to bring the theoretical absorption spectrum more in agreement with experiment. The agreement with theory and experiment will be better in the high-energy region, whereas it will be lower on the low-energy side of the main peak around 8 eV.

In the case of the reflectivity spectra shown in Fig. 8, the agreement between theory and experiment is better than in the case of the dielectric function. This holds especially for the spectral shape, but also for the absolute values of the reflectivity for Si, SiC (comparing with results of Ref. 49 only), and C, omitting the QP corrections. When the QP shifts are included the main peaks in the theoretical and experimental reflectivity spectra fall together. However, a reduction of the reflectivity appears at the low-energy side of the main peaks. The reason is the automatic reduction of the real part of the macroscopic dielectric function in this region. One may speculate that, after inclusion of the electron-hole Coulomb attraction, this failure could be lifted.

D. Energy-loss function

In Fig. 9 we present the results for the electron energy loss (EEL) function ($-\mathrm{Im}[1/\varepsilon^M(\omega)]$) for C, SiC, and Si. The spectra have been obtained within the approach described in Sec. II. Influences of LF and XC effects, as well as quasiparticle corrections of the Kohn-Sham energies on the plasma resonances, are also shown. The influence of the nonlocal contribution to the optical transition operator due to the nonlocality of the pseudopotentials[6] is not indicated in Fig. 9. The calculated energy position of the volume plasmons are presented in Table III in comparison with available experimental results. We find that the use of the momentum opera-

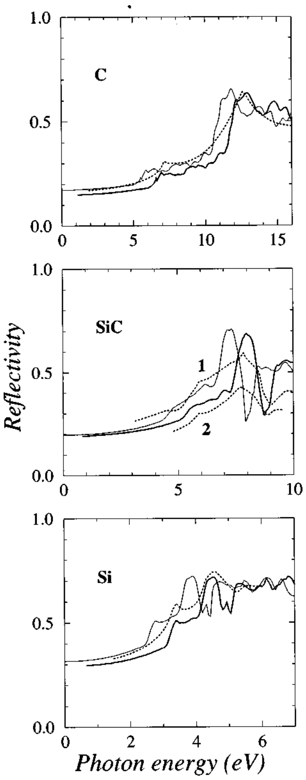

FIG. 8. Comparison of theoretical reflectivity curves (thick solid lines: including LF, XC, and QP effects; thin solid lines: without LF, XC, and QP effects) with measured ones (dotted lines) for Si (Ref. 48), SiC (1) (Ref. 51), SiC (2) (Ref. 52), and C (Ref. 53).

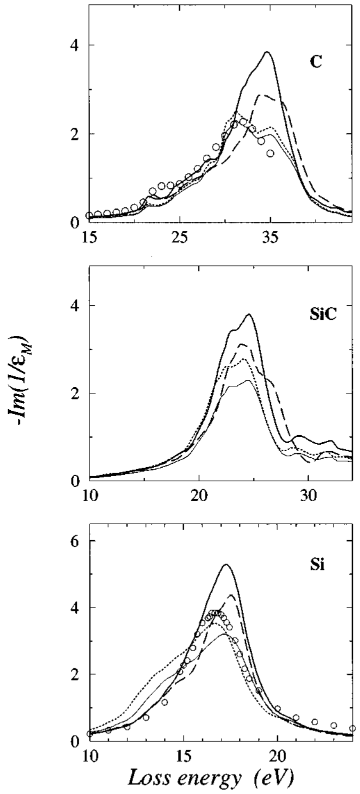

FIG. 9. Electron-energy-loss function for diamond, silicon carbide, and silicon vs loss energy. Bold solid lines: without LF, XC, and QP effects; thin solid lines: with LF effects, dashed lines: with LF and XC effects; dotted lines: with LF, XC, and QP effects. Experimental data (circles) are taken from Refs. 54 (Si) and 55 (C).

tor $\mathbf{p}/m$ instead of the full $\mathbf{v}$ operator in the calculations of the polarization function [cf. Eq. (4)] produces large errors in EEL spectra as compared with experimental data. Without the inclusion of nonlocality effects, the spectral position of the maximum of the EEL function is found at higher (by about 1 eV) energies, and the amplitude of the plasma resonance occurs higher by at least factors 2 or 3 than expected from experiment. The reasons for these findings are errors made in the calculations of the oscillator strengths, and, as a consequence, the violation of the f-sum rule by neglection of the nonlocality of the total Hamiltonian. The changes are most pronounced in the case of silicon. This point was studied in more detail in Ref. 6 for the case of the dielectric function itself.

After inclusion of the nonlocal contribution to the velocity operator, the intensity and spectral position of the maximum of the EEL function approach experimental values, at least for Si and C, where such data are available. Local-field effects strengthen this trend. As it follows from the Fig. 9, influence of the local fields leads to reduction of the intensity, broadening, and shifts of the plasma resonance curves in particular on the low-energy side. However, changes in the intensities and broadenings are overestimated. Unfortunately the spectral position of the EEL function moves somewhat toward higher energies as compared as with the experimental position (see Table III). We mention that our results for plasma resonance in Si agree reasonably with those reported in Ref. 4, where a similar approach has been used. Inclusion of XC moves the curves slightly toward lower energies, and somewhat enhances the intensity of the plasma resonance. The position of the maximum is improved, whereas the intensity of the losses at the low-energy side is futher increased. The incorporation of QP correction moves the EEL curves toward higher energies, in disagreement with experiment. However, the reduction of the broadening of the plasma resonance somewhat improves agreement with experimental data (see Fig. 9). The effects described are qualitative similar on all the materials studied by us, and are most prominent for Si.

V. CONCLUSIONS

We have studied the influence of local-field effects and exchange-correlation corrections beyond the RPA on the optical properties of group-IV materials in the framework of an *ab initio* density-functional method. We find that (i) these

TABLE III. Dependencies of the energies (in eV) of the volume plasmons on LF and XC effects as well as on wave-vector- and band-index-dependent QP corrections in Si cubic SiC and diamond. Starting point is the diagonal approximation. Experimental values are taken from Refs. 54 (SiC and Si) and 55 (C).

Material	diagonal	+LF	+LF+XC	+LF+XC+QP	Expt.
Si	17.28	17.17	17.05	17.69	16.9
SiC	23.71	22.71	22.54	23.83	22.1
C	34.11	32.50	32.41	32.89	32.0

effects do not shift the prominent peak positions in Im $\varepsilon^M(\omega)$ and the zeros in Re$\varepsilon^M(\omega)$, and that (ii) agreement of theory and experiment may be improved in the high-energy regions above the E_1 peaks. However, on the low-energy side the agreement between theoretical Im$\varepsilon^M(\omega)$ spectra with experimental findings will be poorer after inclusion of these effects. We found a weakly pronounced chemical trend. With rising electron localization the influence of LF and XC decreases slightly. Concerning the energy-loss spectra, we state that incorporation of LF and XC effects improve the agreement between theory and experiment.

The influence of quasiparticle corrections is checked using wave-vector- and band-index-dependent self-energy shifts. We observe an obvious remarkable overestimation of these shifts. To bring the peak position in theoretical and experimental spectra closer together smaller quasiparticle shifts are needed.

In order to bring theoretical absorption spectra in the low-energy region closer together with measured line shapes, i.e., near to the onset of the absorption, we suggest that excitonic effects have also to be included in the *ab initio* calculations. The dynamical treatment of the electron-hole attraction could be also a step toward explaining why renormalizations of the quasiparticle strengths do not play practically any role.

ACKNOWLEDGMENTS

We thank W. van Haeringen, R. Del Sole, and V. Sahni for useful discussions and comments on the manuscript. We are indepted to P. Käckell and W.G. Schmidt for their help with the computer codes. Some modules of the computer code were taken from a program for the description of optical properties without local fields developed together with B. Adolph and K. Tenelsen. This work was financially supported by the Deutsche Forschungsgemeinschaft (SFB 196, Project No. A8), and the EC Programme Human Capital and Mobility (Contract No. ERBCHRXCT 930337).

---

[1] C. S. Wang and B. M. Klein, Phys. Rev. B **24**, 3471 (1981).

[2] M. Alouani, L. Brey, and N. E. Christensen, Phys. Rev. B **37**, 1167 (1988).

[3] Z. H. Levine and D. C. Allan, Phys. Rev. Lett. **63**, 1719 (1989); Phys. Rev. B **43**, 4187 (1991); **42**, 3567 (1990); **44**, 12 781 (1991).

[4] R. Daling, W. van Haeringen, and B. Farid, Phys. Rev. B **45**, 8970 (1992).

[5] K.-H. Lee, C. H. Park, B.-H. Cheong, and K. J. Chang, Solid State Commun. **92**, 869 (1994).

[6] B. Adolph, V. I. Gavrilenko, K. Tenelsen, F. Bechstedt, and R. Del Sole, Phys. Rev. B **53**, 9797 (1996).

[7] H. Ehrenreich and M. H. Cohen, Phys. Rev. **155**, 786 (1959).

[8] S. L. Adler, Phys. Rev. **126**, 413 (1962).

[9] N. Wiser, Phys. Rev. **129**, 62 (1963).

[10] P. Hohenberg and W. Kohn, Phys. Rev. **136**, B864 (1964).

[11] W. Kohn and L. J. Sham, Phys. Rev. **140**, A1133 (1965).

[12] R. Del Sole and R. Girlanda, Phys. Rev. B **48**, 11 789 (1993).

[13] J. P. Walter and M. L. Cohen, Phys. Rev. B **2**, 1821 (1970).

[14] J. A. Van Vechten and R. M. Martin, Phys. Rev. Lett. **28**, 446 (1972).

[15] S. G. Louie, J. R. Chelikowsky, and M. L. Cohen, Phys. Rev. Lett. **34**, 155 (1975).

[16] W. Hanke and L. J. Sham, Phys. Rev. B **21**, 4656 (1980).

[17] C. E. Pickett, Comments Solid State Phys. **12**, 57 (1985).

[18] W. Hanke, Adv. Phys. **27**, 287 (1978).

[19] T. W. Josefsson and A. E. Smith, Aust. J. Phys. **46**, 635 (1993).

[20] A. Baldereschi and E. Tosatti, Phys. Rev. B **17**, 4710 (1978).

[21] P. E. Van Camp, V. E. Van Doren, and J. T. Devreese, Phys. Rev. B **24**, 1096 (1981).

[22] J. Chen, Z. H. Levine, and J. W. Wilkins, Phys. Rev. B **50**, 11 514 (1994).

[23] S. Baroni and R. Resta, Phys. Rev. B **33**, 7017 (1986).

[24] M. S. Hybertsen and S. G. Louie, Phys. Rev. B **34**, 5390 (1986).

[25] M. S. Hybertsen and S. G. Louie, Phys. Rev. B **35**, 5585 (1987).

[26] S. de Gironcoli, S. Baroni, and R. Resta, Phys. Rev. Lett. **62**, 2853 (1989).

[27] W. R. L. Lambrecht and B. Segall, Phys. Rev. B **40**, 7793 (1989).

[28] A. Dal Corso, S. Baroni, and R. Resta, Phys. Rev. B **49**, 5323 (1994).

[29] H. Ehrenreich, in *The Optical Properties of Solids, Proceedings of the International School of Physics ''E. Fermi,''* edited by J. Tauc (Academic, New York, 1966).

[30] H. Bross, O. Belhachemi, B. Mekki, and A. Seoud, J. Phys. Condens. Matter **2**, 3919 (1990).

[31] D. L. Johnson, Phys. Rev. B **9**, 4475 (1974).

[32] G. D. Mahan, *Many-Particle Physics*, 2nd ed. (Plenum, New York, 1990), Chap. 4 and 5.

[33] S. P. Singhal and J. Callaway, Phys. Rev. B **14**, 2347 (1976).

[34] R. M. Martin and K. Kunc, in *Ab Initio Calculations of Phonon Spectra*, edited by J. T. Devreese, V. E. Van Doren, and P. E. Van Camp (Plenum, New York, 1983), p. 49.

[35] A. Zangwill and P. Soven, Phys. Rev. A **21**, 1561 (1980).

[36] R. M. Pick, M. H. Cohen, and R. M. Martin, Phys. Rev. B **1**, 910 (1970).

[37] For this particular case explicit representations of the velocity operator are given in Refs. 6 and 25.

[38] R. Stumpf and M. Scheffler, Comput. Phys. Commun. **79**, 447 (1994).

[39] L. Kleinman and D. M. Bylander, Phys. Rev. Lett, **48**, 1425 (1982).

[40] P. Käckell, B. Wenzien, and F. Bechstedt, Phys. Rev. B **50**, 17 037 (1994).

[41] *Semiconductors, Physics of Group IV Elements and III-V Compounds*, edited by O. Madelung, Landolt-Börnstein, New Series, Group III, Vol. 17, Part a (Springer, Berlin, 1982)

[42] F. Bechstedt, R. Del Sole, G. Cappellini, and L. Reining, Solid State Commun. **84**, 765 (1992).

[43] G. Cappellini, R. Del Sole, L. Reining, and F. Bechstedt, Phys. Rev. B **47**, 9892 (1993).

[44] B. Wenzien, P. Käckell, F. Bechstedt, and G. Cappellini, Phys. Rev. B **52**, 10 897 (1995).

[45] D. M. Ceperley and B. J. Adler, Phys. Rev. Lett. **45**, 566 (1980).

[46] J. P. Perdew and A. Zunger, Phys. Rev. B **23**, 5048 (1981).

[47] D. Jepsen and O. K. Anderson, Solid State Commun. **9**, 1763

(1971); G. Lehmann and M. Taut, Phys. Status Solidi **54**, 469 (1972).

[48] D. E. Aspnes and A. A. Studna, Phys. Rev. B **27**, 985 (1983).

[49] S. Logothetidis, H. M. Polatoglou, J. Petalas, D. Fuchs, and R. L. Johnson, Physica B **185**, 389 (1993).

[50] A. D. Papadopoulos and E. Anastassakis, Phys. Rev. B **43**, 5090 (1991).

[51] B. E. Wheeler, Solid State Commun. **4**, 173 (1966).

[52] W. R. Lambrecht, B. Segall, M. Yoganathan, W. Suttrop, R. P. Devaty, W. J. Choyke, J. A. Edmond, J. A. Powell, and M. Alouani, Phys. Rev. B **50**, 10 722 (1994).

[53] W. C. Walker and J. Osantovski, Phys. Rev. A **134**, 153 (1964).

[54] H. Raether, *Excitation of Plasmons and Interband Transitions by Electrons.* Springer Tracts in Modern Physics Vol. 88 (Springer, New York, 1980).

[55] H. R. Phillips and E. A. Taft, Phys. Rev. **136**, A1445 (1964).